Master's thesis

NTNU
Norwegian University of Science and Technology
Faculty of Information Technology and Electrical Engineering
Department of Electronic Systems

Svein Kristian Rougseth

Local magnetic field device for artificial spin ice

Master's thesis in Electronics Systems Design and Innovation
Supervisor: Erik Folven
Co-supervisor: Jakob Vinje
June 2021

NTNU
Norwegian University of
Science and Technology

Svein Kristian Rougseth

Local magnetic field device for artificial spin ice

Master's thesis in Electronics Systems Design and Innovation
Supervisor: Erik Folven
Co-supervisor: Jakob Vinje
June 2021

Norwegian University of Science and Technology
Faculty of Information Technology and Electrical Engineering
Department of Electronic Systems

NTNU
Norwegian University of
Science and Technology

Abstract

An artificial spin ice is a system that is made up of a collection of coupled dipole nanomagnets. Although the magnets individually do not behave in any special way, the lattice as a whole has a range of complex and interesting behaviors. In the last decade, they have been the subject of a significant amount of research, as they have potential applications across many industries.

One application which is especially relevant for this work is computing. Artificial spin ices have been suggested as candidates for low-power and reservoir computing, as they can be tailored to have very complex responses to a given input signal. To use them in this fashion, a signal has to be applied to the input of the system, and this work will examine a method for doing this.

As the magnets are tightly coupled, changing the magnetization direction of a nanomagnet will affect its neighbors, and propagate throughout the lattice. This can be done by applying a magnetic field to the magnet, typically by using a powerful external magnet. This work examines whether it is possible to use a simple wire, or a *stripline*, as a small magnetic field generator which affects only one or a small group of nanomagnets.

The properties of the stripline and the magnetic field were initially investigated through simulations using Comsol® Multiphysics. The simulations showed that a stripline can be manufactured which is of a suitable size for the deposition of nanomagnets, while still generating a sufficient magnetic field with a reasonable current supply.

The results of the simulations were used to manufacture samples at NTNU Nanolab, which were tested for current capacity and inspected under magnetic force microscopy. Due to manufacturing problems, the samples were not suitable for measurement of the magnetic field strength, so the simulation results still require verification.

Sammendrag

En kunstig spinn-is er en er et system som består av en sampling koblede dipolmagneter. Individuelt har magnetene en helt vanlig oppførsel, men kollektivt utøver de en rekke komplekse og interessante oppførsler. I det siste tiåret har disse systemene vært et aktivt forskningstema, ettesom de har mulige bruksområder på tvers av mange industrier.

Et bruksområde som er spesielt relevant for dette arbeidet er beregning. Kunstig spinn-is kan være en passende kandidat for lavstrøms- eller reservoar-beregning, ettersom de kan produseres slik at de har en ekstremt kompleks respons til et gitt inngangssignal. For å kunne brukes til dette må det være mulig å påtrykke signaler på inngangen av dette systemet, og dette arbeidet undersøker en metode for å gjøre nettopp dette.

Ettersom magnetene i isen er veldig tett koblet, vil det å endre magnetiseringsretningen til en magnet også påvirke de nærliggende magnetene, noe som vil bre seg videre utover i gitteret. Magnetene kan snus ved å påtrykke et magnetfelt, typisk ved bruk av en sterk ekstern magnet. Dette arbeidet vil se på hvordan dette heller kan gjøres med det lokale magnetfeltet fra en leder, slik at man kan snu en enkeltmagnet eller en gruppe magneter.

I første omgang ble lederens egenskaper undersøkt via simuleringer i Comsol® Multiphysics. Simuleringene viste at at det er mulig å produsere en leder har dimensjoner som gjør det mulig å generere et magnetfelt av passende størrelse med rimelig strøm, mens den fortsatt er stor nok til å deponere nanomagneter oppå.

Resultatene fra simuleringene ble brukt til å produsere et sett med prøver på NTNU Nanolab, som ble testet for strømkapasitet og inspisert med magnetisk domenavbildning. Grunnet produksjonsvanskeligheter var ikke prøvene brukbare for karaktisering av feltstyrken, så simuleringene krever fortsatt verifisering.

Preface

This master thesis is the conclusion of a five year study in *"Electronic systems design and innovation"* at the Norwegian University of Science and Technology. It was performed at the Department of Electronic Systems for the electron oxide group, under the supervision of associate professor Erik Folven and postdoc Jakob Vinje.

License

Acknowledgements

Many people assisted me in this work, and without their help, I would have barely known where to start. Erik Folven, Jakob Vinje, Anders Strømberg and Rune Strømholt have all helped me greatly with training, methods and ideas, and I would surely still be scratching my head if it were not for them.

I greatly appreciated having Erik as my supervisor, it has been a joy to have such a fun, clever and kind person to guide me this past semester.

Finally, special thanks go out to Jakob, who took great amounts of time out of his schedule to assist in all things, and whose great skill with a pair of tweezers is an inspiration to us all.

Contents

Acronyms

3DR	3D Rotator
AC	alternating current
AFM	atomic force microscopy
ASI	artificial spin ice
DC	direct current
DIW	distilled water
EBL	electron-beam lithography
FEM	finite element method
IPA	isopropanol
LCC	leadless chip carrier
MFM	magnetic force microscopy
MLA	maskless aligner
PEB	post-exposure bake
Py	permalloy
SEM	scanning electron microscope
SMU	source measure unit

Symbols

Symbol	Description	Unit
$\vec{B}$	magnetic flux density	T
$\vec{H}$	magnetic field strength	A/m
$\vec{H}c$	magnetic switching field strength	A/m
M_s	coercitivity	A/m
$\vec{D}$	electric displacement field	C/m^2
$\vec{E}$	electric field	V/m
E	total free energy	J
E_{an}	anisotropy energy	J
E_{ex}	exchange energy	J
E_{Z}	zeeman energy	J
E_{d}	demagnetizing energy	J
E_{s}	strain energy	J
E_{ms}	magnetostriction energy	J
I	current	A
$\vec{J}$	current density	A/m^2
ϵ_0	electric permittivity of free space	F/m
μ_0	magnetic permeability of free space	H/m
P	power	W
R	resistance	Ω

1 Introduction

In the last decade, the fundamental paradigm which has been driving the increase in computing power since the first transistor is being pushed to its limits. According to the IRDS 2020 report, the current state of the art mass-produced systems are finFET systems, onward to lateral gate-all-around devices, eventually extended to 3D architectures. It predicts that after 2034, MOSFET scaling is unlikely to yield significant improvements, and "Beyond CMOS" technologies may enter the mainstream production process.

This has led to an increasing interest in alternative materials and methods of creating processing systems, such as quantum computing, single-atom transistors, and spintronics. One topic which is the subject of some research are *artificial spin ices (ASIs)*, where a lattice of nanoscale magnets are laid out in a tight pattern. The magnets are dipole coupled and thus have magnetization directions which depend on the nearby magnets. This causes a complex response which propagates throughout the entire lattice, making them potentially useful in applications like reservoir computing, and possibly even as logic gates or memory.

1.1 Structure of this document

This document consists of three parts: An introduction and some background will be given from chapter 1.2 to chapter 3, this part contains an introduction to the project and the underlying theory. Chapter 3 explains the methods and procedures which will be used for ssimulationand fabrication. Finally, chapter 4 presents and discusses the results.

1.2 Motivation & goals

In any application of ASIs in computational systems, we are interested in the propagation of signals through the lattice. Some applications do not care about the internal mechanics, only the relation between the input and the output, while other applications attempt to tailor the size and position of the nanomagnets to perform a certain task.

To be able to practically use the ASI for a purpose such as these, one must be able to apply and read out signals. This work will consider the task of applying signals, and examine the design and fabrication of a microscale structure which can switch the magnetization direction of the nanomagnets by generating a local magnetic field.

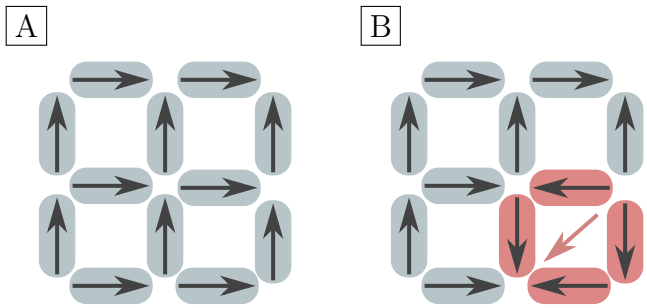

Figure 1: A top-down illustration of some magnetic islands in a square ASI. A shows them magnetized in some arbitrary initial direction. B shows a magnetic field being applied at an angle to change the magnetization directions of one group of nanomagnets.

For this we need a small magnetic field of approximately 46 mT along the length of the nanomagnets [1]. This work will focus on flipping single nanomagnets only, however, by increasing the width of the structure,

The device that converts current to EM-fields is called an electromagnet. A typical design for this type of device is what is known as a *field coil*, which is typically manufactured by winding resist-coated copper wire around a ferrite core. As the strength of the field increases with the number of turns of the coil, they produce large fields with low current.

For micrometer scale coils, the classical manufacturing method is impractical, however, lithography can be used to manufacture similar structures, such as the one in figure 2. This coil can be made by depositing two separate layers, one copper layer for the coil, and a ferromagnetic layer as the core.

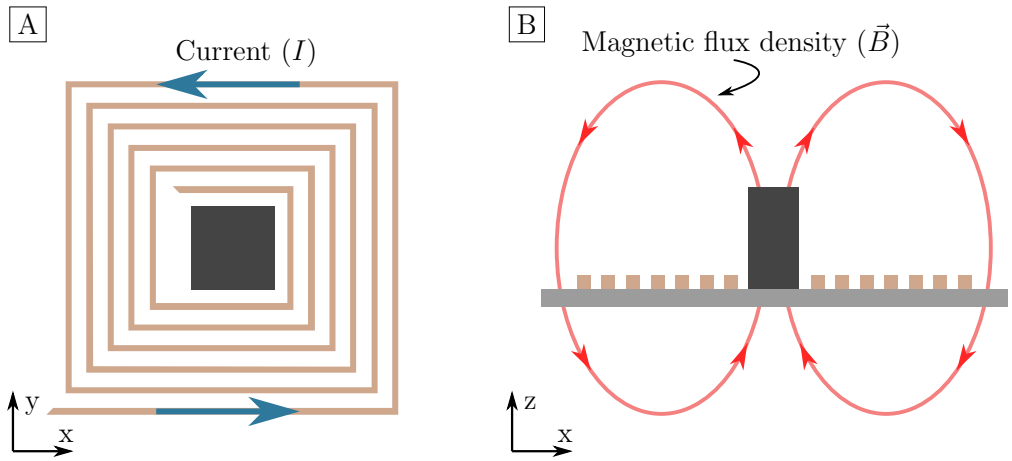

Figure 2: An illustration of a typical structure for a field coil, adapted for lithography. Note that as the current runs around the core, the magnetic field lines pass out of the core, around the structure, and back into the other side of the core. A is seen from the top, while B is a cross-section seen from the side

Our specific use case will require a different design. To flip the nanomagnets, the magnetic field must be aligned along them. There is no convenient location to place the nanomagnets so that the magnetic field runs parallel to them with this design, as the magnetic field is out-and-in of plane.

A design that mitigates this, and is also the simplest electromagnet that can be made, is a straight wire, or what is commonly referred to as a *stripline*. This is usually used as a waveguide in electrical applications, however, we only need it to carry current. As there are no windings, the current required to generate a given field strength is much higher than what it would be using a typical electromagnet, and the field is directed across it, so we will have to deposit the nanomagnets directly onto the stripline.

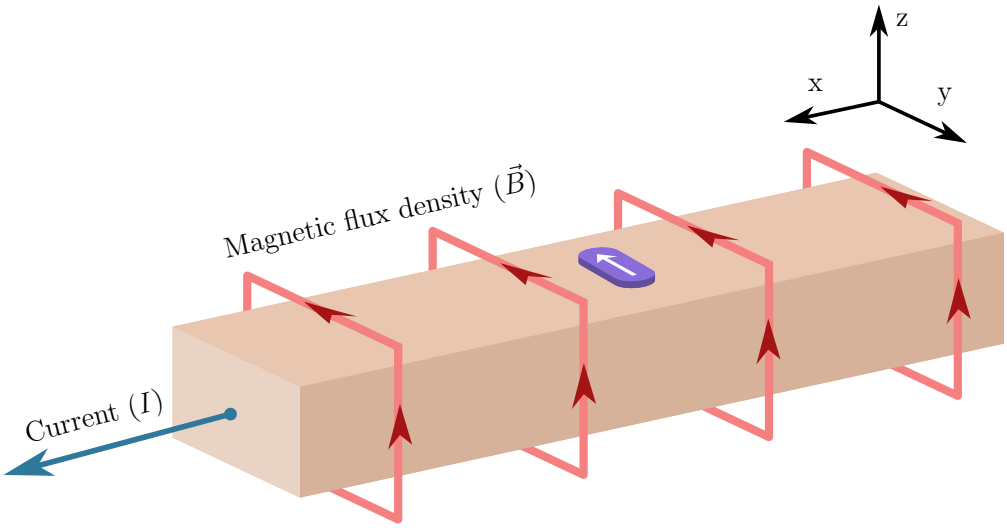

Figure 3: An illustration of the operation of a stripline as an electromagnet. As current is run through the stripline, a magnetic field loops around it with a strength proportional to the current. A nanomagnet is deposited directly on the metal so that the magnetic field is aligned along it.

2 Background

This chapter will present some of the theoretical background of the project. A short introduction to micromagnetics will be given to help understand the nanomagnets and their operation. Additionally, some short descriptions and equations will be presented on resistive heating and electromagnetism, which will be used in the simulations.

2.1 Artificial spin ice

Artificial spin ices (ASIs) are structures of magnetically coupled dipole magnets, which have properties not normally present in the material. Although this thesis does not directly involve ASI, it is where the inspiration comes from, and forms the basis for many assumptions and choices. For this reason, a short introduction to the topic will be given here. Further reading on the topic includes "Frustrated Materials and Ferroic Glasses" [2], which gives a more in-depth explanation, and "Advances in artificial spin ices" [3], which is a good source of information on the current state of the art.

An ASI is fundamentally only a group of dipoled coupled magnetic islands. Each magnet has a well-defined north pole and south pole, and due to their proximity, is coupled to nearby magnets. This, in the sense that there is a tension between the magnets in the ASI, is called *frustration*.

One of the fundamental mechanics of an ASI is due to the fact that the north pole and south pole can flip to reduce the energy state of the local group of magnets. If the thermal energy is sufficient. This happens spontaneously, which propagates throughout the lattice and leads to the ASI settling into the lowest available energy state, or *ground state*. Some different types of ASIs and their ground states are shown in figure 4.

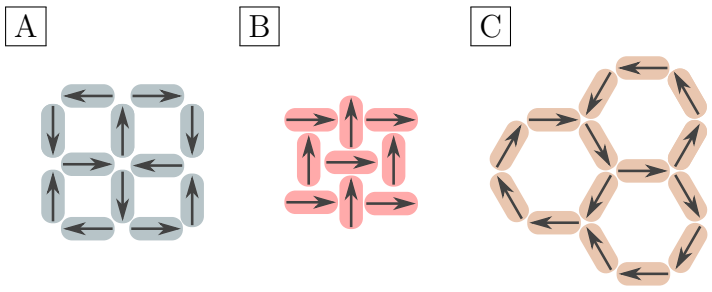

Figure 4: Square ASI A, pinwheel ASI B and Kagome ASI C. Illustrated as a top-down view of nanoscale magnets, with arrows to indicate magnetization direction.

By upsetting the ground state, for example by switching a nanomagnet, cascade reactions can be initiated, in which the change in state propagates throughout the entire lattice.

2.2 Micromagnetic interactions and domains

This thesis will examine the generation of magnetic fields to flip the magnetization direction of the magnets in an ASI. To help understand this topic, this chapter will give a brief introduction to micromagnetics and the origin of micromagnetic structures. For more information on this topic, the reader is encouraged to refer to "Magnetism and magnetic materials" by J. M. D. Coey[4], which is the source of much of the following information.

On a large scale, such as on fridges or cars, magnets will attract and align based on their magnetic properties. Our intuition tells us that two magnetic poles will repel each other if they are equal, and attract each other if they are opposite.

This behaviour of a magnet as a whole is a result of the behaviour of the magnetic moments within. In materials that are typically considered "magnetic", the atomic structure is such that the magnetic moments will align spontaneously, so long as the temperature is low enough. This property is called *ferromagnetism*, and is relatively rare among naturally occurring substances. Until modern times, essentially all known ferromagnetic metals were primarily an alloy of iron, cobalt, or nickel, and these still make up a large portion of common ferromagnetic metals today [4, ch. 1, 5, 11].

Everyday magnets, such as fridge magnets or bar magnets, are all *permanent magnets*, which have all magnetic moments pointing in the same direction. This is not typically the state materials exist in, instead, they are organized in large groups which point in roughly the same random direction. To all point the same way, they have to be coerced, or *magnetized*, by an external field. The energy required to do this depends on the material, and is described by the *coercitivity* (M_s) factor. Naturally, a high coercitivity is a desired property in a permanent magnet, as, even though initially magnetizing it is harder, it will have a smaller chance of being demagnetized over time.

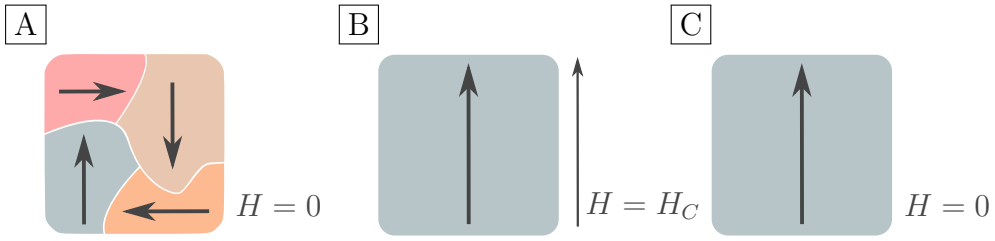

Figure 5: Illustration of a cross section of a ferromagnetic material. A Several large domains have formed as the nearby magnetic moments have aligned. After an external magnetic field H_c of sufficient strength is applied, all magnetic moments have been magnetized along the field B, and will remain magnetized in this direction after the field is gone C

.

If the coercitivity is very large, the material is commonly called a *hard* ferromagnet, in the sense that a large magnetic field is required to magnetize it. In the same fashion, a *soft* ferromagnet has a low coercitivity, and is easier to magnetize. For the most part, only hard ferromagnets can be used to create permanent magnets, as soft ferromagnets will spontaneously form distinct internal domains with different magnetization directions.

The domains form to minimize the total free energy (E) of the system. If the ferromagnet is magnetized in only one direction, there is a large energy cost associated with maintaining a large outward, or *stray*, field. To reduce the size of this field, the domains along the edges of the material will form loops, as is illustrated in figure 6.

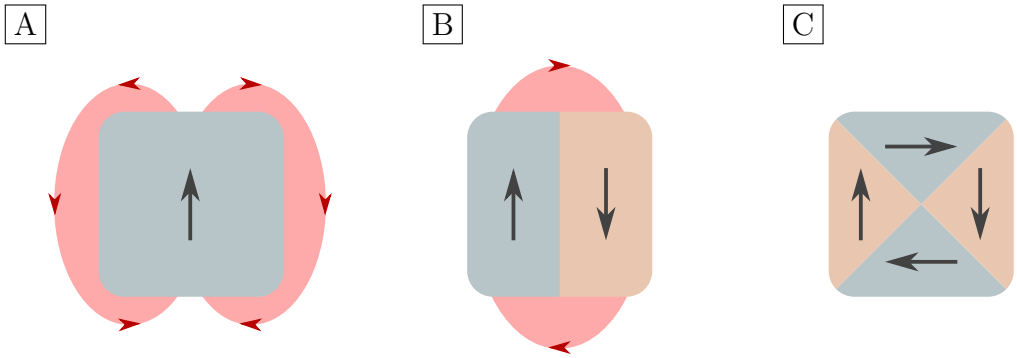

Figure 6: Illustration of three possible configurations of a small magnet. A single magnetic domain A, two opposing domains which reduce the size of the stray field B and a full loop which eliminates the stray field C. C is the most stable configuration, as it has the smallest stray field.

The total free energy is a sum of several factors relating to the material and the forces upon it, and is expressed as [4, p.234]

$$E = E_{\text{ex}} + E_{\text{d}} + E_{\text{an}} + E_{\text{Z}} + E_{\text{s}} + E_{\text{ms}}, \tag{1}$$

where E is the total free energy, E_{ex} is the exchange energy, E_{d} is the demagnetizing energy, E_{an} is the anisotropy energy, E_{Z} is the zeeman energy, E_{s} is the strain energy, and E_{ms} is the magnetostriction energy.

The exchange energy (E_{ex}) increases the energy cost of having electrons which are not aligned with neighboring electrons. It arises from a combination of the *Pauli exclusion principle*, which for electrons states that no two electrons with the same spin may occupy the same location, and the electrical repulsion between the electrons. This effect is purely quantum mechanical and the explanation is mostly mathematical, so the details will not be discussed here, but more information can be found in chapter 5.2 in "Magnetism and magnetic materials"[4].

The demagnetizing energy (E_{d}) is the energy cost of maintaining the stray field, and dominates at micrometer scales. This is one of the primary drivers of domain formation, as forming multiple domains which form a loop eliminates the stray field.

Often some of these energy contributions are negligible, depending on the material and the forces acting on it. For our use case, the anisotropy energy (E_{an}), strain energy (E_{s}) and magnetostriction energy (E_{ms}) are very small, as permalloy (Py) has a very small anisotropy energy [5], and there are no external forces applied to the magnets. Lastly, the zeeman energy (E_{Z}) is the energy cost of not aligning with an externally applied magnetic field, which will be used to switch the magnetization direction of the magnets.

2.3 Nanomagnets

The ASI requires magnets which are *dipole coupled*, which means that the magnets are required to have a well-defined north and south pole and a strong stray field. To create magnets which behave this way, we have to eliminate the magnetic domains which form loops and reduce the stray field.

This is done by reducing the dimensions of the magnetic material. When the radius of the island drops below roughly 100 nm, the exchange energy surpasses the demagnetization energy, and we begin to see monodomain magnets. These magnets do not have multiple separate domains with different magnetization directions, but instead have all magnetic moments pointing in roughly one direction, and are called *nanomagnets*.

The magnetization direction of this domain is dependent on the *shape anisotropy* [4, p. 265], which is a property where a magnet is easier to magnetize in some directions than others. The shape anisotropy is a consequence of the anisotropy energy and demagnetizing energy of different magnetization directions, which can be illustrated as a build-up of "magnetic charges" [1] on the surface of the magnet. For an elliptical shape, the surface area is smaller when magnetized along the length of the magnet than it is when magnetized perpendicular to it, as illustrated in figure 7.

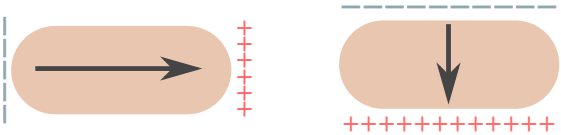

Figure 7: Illustration of a top-down view of two identical magnets at nanometer scales. Magnetization along the length of an elliptical magnet leads to a lower build up of "magnetic charges" than magnetization perpendicular to the length.

This can be utilized to create nanomagnets with different properties by tailoring its dimensions. Ellipsis nanomagnets have only two stable magnetization directions, making them suitable for ASI, where the frustration between the magnets is essential. Circular magnets are symmetrical, and so can magnetize in any direction, and can be used as a compass to detect and store the direction of an applied magnetic field. Square nanomagnets have 8 possible magnetization directions, and can for example be placed between the elliptical ones in an ASI as a "pick-up" magnet to encode the nearby magnetization states. [6].

Figure 8: An illustration of a top-down view of several different shapes and magnetization directions for different shapes of nanomagnets.

[1] Magnetic charges do not exist, but they are useful to visualize this effect

This work will focus mainly on 220 nm × 80 nm × 10 nm elliptical nanomagnets made of Py with a 2.5 nm Ti cap, as these have been found to have switching energy of 46 mT ± 2 mT [1].

2.4 The Oersted field / Ampéres Law

The mechanism which will be used to switch the magnetization direction of the nanomagnets, is the *Oersted field*.

The Danish physicist Hans Christian Ørsted/Oersted is credited with discovering the relation between electric currents and magnetic fields. He observed that a needle suspended in water would initially align with the earth's magnetic field, and rotate roughly 45° as current was run through a nearby wire.[7, 8]

The relation between current and electromagnetic fields is governed mathematically by *Ampéres law*, which is expressed in a simplified form as

$$\oint \vec{B} \cdot dl = \mu_0 I, \tag{2}$$

with l being the rotation about the wire [4, p. 30]:

The physical interpretation of this equation is that a current through a wire generates a magnetic field which loops around the wire, and in theory, we can use this to calculate the field generated by any given current.

In practice, this simplified formula, while a good example for understanding the interpetation of the mathematics, is a little too simplified to be useful for our geometry. This is primarily because this formula assumes that the current passes through an infinitely thin conductor, thus only applies when the scale of the system is significantly larger than the width of the wire.

If instead of multiplying by the total current I, the current density $\vec{J}$ is integrated over a cross-section S, we get

$$\oint \vec{B} \cdot dl = \iint_S \mu_0 \vec{J} \, \mathrm{d}\vec{s}, \tag{3}$$

which makes it possible for us to calculate the magnetic field for inhomogenous current distributions and systems where the conductor is relatively large. This equation, on differential form, is what will be used in simulations.

Because he discovered the relation between magnetic fields and electric currents, and because it is a convenient name, this field will be referred to as the *Oersted field* in this work.

2.5 Resistive heating

When a current passes through a wire, it generates heat. As the current density will be quite high in this project, a concern is that the wire will melt due to the resistive heating.

This is due to two effects, induction heating and direct resistive heating. Induction heating is for the most part only relevant in high-current alternating current (AC) applications, such as an induction oven, while resistive heating is present in all electrical systems[9, p. 2].

In general, we say that the the power disipation of a resistor from direct resistive heating is given as [10, pp. 834]

$$P = I^2 R.$$

As a metal heats up, its properties change. For a conductor, the resistivity will increase as the temperature increases, for a semiconductor it will decrease, and for a superconductor, the resistivity will be 0 below a certain temperature. [10, pp. 823-824]

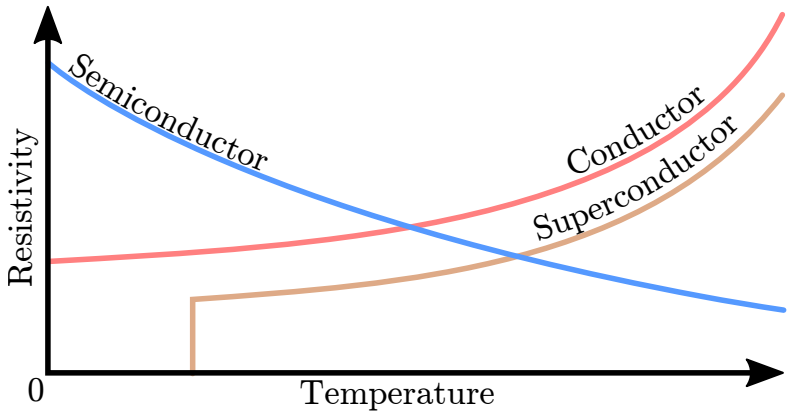

Figure 9: Schematic representation of resistivity characteristic of different materials. The semiconductor has a steadily decreasing resistivity with temperature, which eventually flattens out. The conductor acts in a similar but opposite fashion, where an increase in the temperature increases the resistivity. The superconductor drops to a resistance of exactly zero below a given temperature.

This creates feedback loops, which can be either negative or positive. If a resistor is powered by a typical voltage supply, the increased resistivity of the resistor will reduce the current, which will reduce the heat output of the resistor. If the power is supplied by a current source, the opposite will happen: The increased resistivity does not reduce the current, so the effect is increased, which in turn increases the heat output. This can eventually cause a burn-out of the resistor, which will destroy the sample.

3 Experimental methods

3.1 Design

The design of the electromagnet has the following constraints:

- Needs to produce a magnetic field strength of at least 46 mT parallel to the long axis of the nanomagnets.
- Has to be able carry the sufficient current without melting
- Sizeable contacts for external connections
- Metal has to be suitable for further deposition of Py
- Dimensions must be large enough to be reliably fabricated with lithography

The design which will be used is shown in figure 10. Two large contact pads taper into the stripline, so that connections can be made to external equipment. A range of sizes of nanomagnets are used in case of unforeseen circumstances.

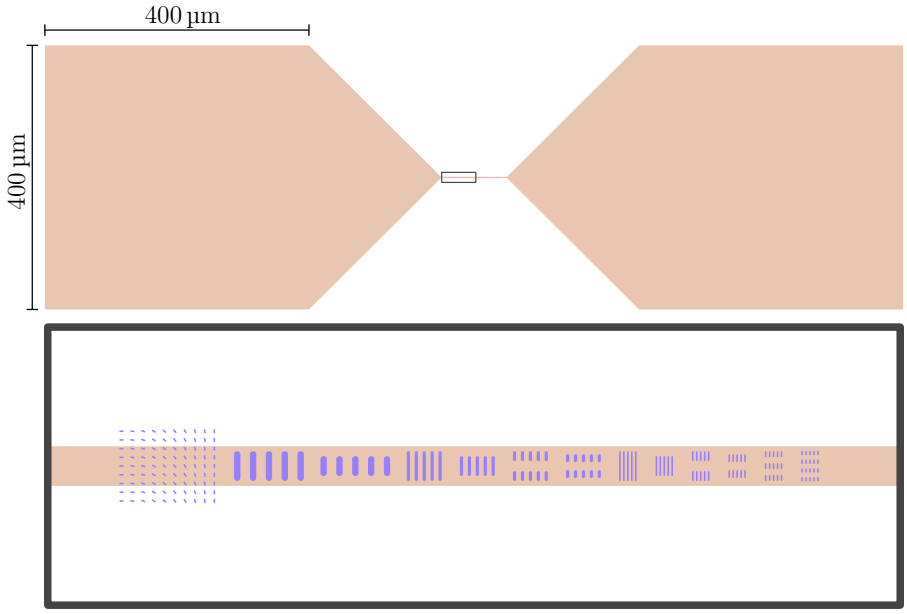

Figure 10: The design of structure. There are two large contact pads, a taper, and a stripline. The parameters of the contacts do not affect the magnetism much, and is fixed at 400 µm. An inset shows a magnification of the stripline, where a range of sizes are deposited directly on the metal.

3.2 Lithography

A short introduction to lithography and the methods used in the chapter on sample fabrication will be provided here, but for further reading,

Lithography is a word which has had many meanings throughout history, as it simply means to "write on stone". In microfabrication, lithography typically refers to *photolithography*, the process of using light to expose patterns on to semiconductor materials. Using this method allows for fabrication of structures which are extremely small, even below the wavelength of light.

Photolithography works by using a light source of a specific wavelength, for example 405 nm, to expose a pattern on a material called *photoresist*. There are many different types of photoresists which react differently to light, but for simplicity, let us consider one which degrades when exposed, or what is known as a *positive* resist. [11, pp. 120, 121]

When the pattern is exposed on the photoresist, and the sample is placed in a suitable chemical called a *developer*, the degraded regions will be dissolved by the developer, leaving a hole down to the substrate in the shape of the pattern. These holes can then, for example, be filled with metal to create conductors, or with an etching agent to carve grooves into the material below. An illustration of filling with metal is illustrated in figure 11.

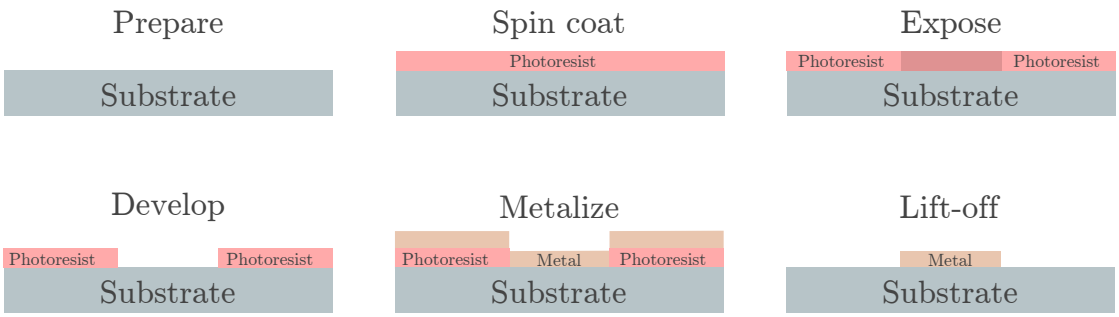

Figure 11: Illustration of process for deposition metal on the substrate, illustrated as cross-section of wafer. For multilayer structures this process can be repeated multiple times

In addition to photolithography, there are other types of lithography methods which try to improve resolution or reliability, notably electron-beam lithography (EBL), which is a maskless lithography process that uses an electron beam instead of light. This method has very high resolution at the cost of being significantly slower, but is convenient for small structures with features that are too small for typical photolithography, for example nanomagnets. [11, p. 46]

3.3 Wirebonding

To interface with the circuitry from the measuring equipment, the sample must be connected to suitable holders. A convenient way of doing this is *wirebonding*, which is a process that adapts ultrasonic soldering for micrometer scale applications. The working principle is similar to soldering, where a metal wire is used to connect to the contact pads, however, the metal is not melted in wirebonding. Instead, a combination of relatively low temperature (typically between 50 °C and 200 °C), downward force and ultrasound is used to form a weld.

Although there exist machines which do this automatically, the one available at NTNU Nanolab is relatively manual, and so, the temperature, force, and ultrasound strength are parameters which must be adapted to the target. Some materials are well suited to wirebonding, such as soft metals which do not form hard oxide layers, and in general, these parameters have to be increased with increasing material hardness. See appendix A for example values.

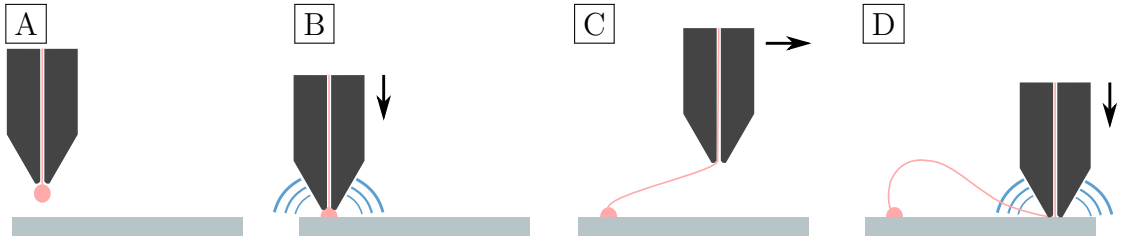

Figure 12: Illustration of wirebonding process. The target is heated, and a length of the wire is melted into a ball A, which is brought down to the surface. A downward force and ultrasound is applied, which bonds the wire to the target B. The wire is brought to the second bond point C, where the same process is done D.

3.4 Atomic and magnetic force microscopy

The structures created in this work will be smaller than the wavelength of visible light, and so are not observable through optical microscopes. Additionally, we would like to examine the magnetic properties of the substrate, which can not be done using typical microscopy. For these purposes, atomic force microscopy (AFM) and magnetic force microscopy (MFM) will be used.

The operating principles for the AFM and MFM are essentially the same. A small cantilever with a measurement tip is extended above the sample, which is deflected by the interaction between the tip and the sample. A laser interferometer reads the distance to the cantilever, which is then used to calculate the distance between the tip and the material.

Depending on the distance between the sample and the tip, and how the values are interpreted, this can be used to measure both the physical dimensions of nanoscale objects, as well as the strength of the stray magnetic in the upwards direction.

3.5 Characterization methods

There are three values which are interesting when characterizing the stripline: The current capacity, resistance, and field strength. Table 3 shows a list of the used instruments, and some of them are shown in figure 13.

Keithley® 2450 SourceMeter®
Attocube® atto3DR sample rotator module
Attocube® attoDRY1000/SU closed-cycle crystat

Table 3: List of used instruments

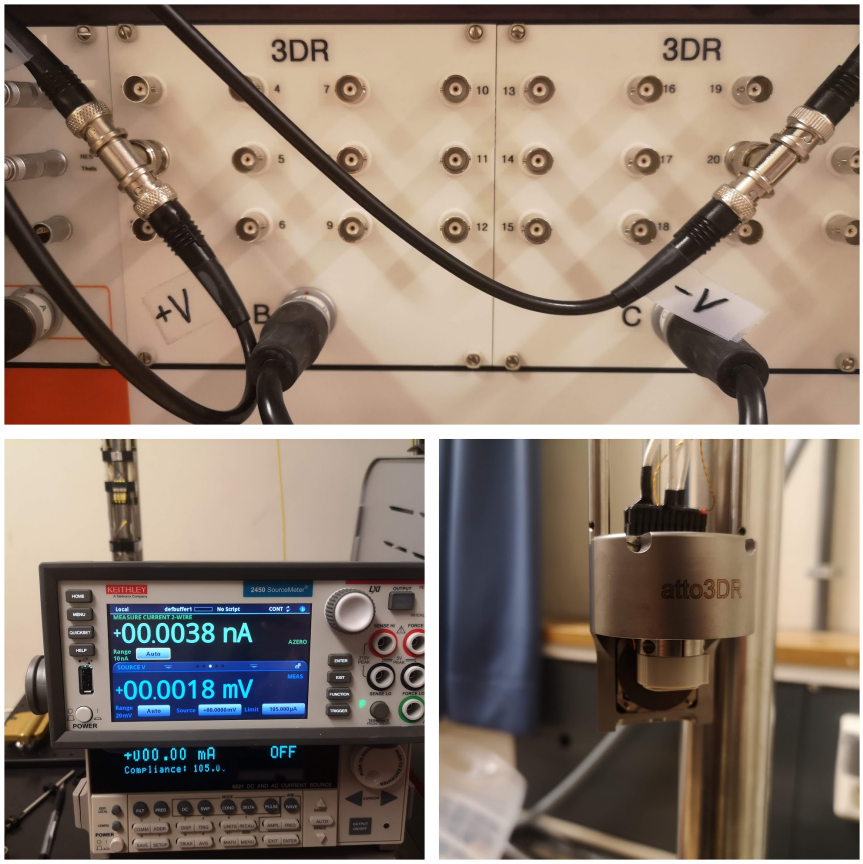

Figure 13: Top: Patchboard, Bottom left: 2450 source measure unit (SMU), Bottom right: Attocube® 3D Rotator (3DR)

For the measurements, the Attocube® 3DR and AFM will house, cool, and communicate with the samples. Signals will be applied and measured using a Keithley® SMU.

The largest stripline widths simulated require up to 700 mA, which is within the limits of what the SMU can supply. There is a caveat to this, which can be seen in the power envelope chart in figure 14, which is that it can only supply this current while the output voltage is below 20V.

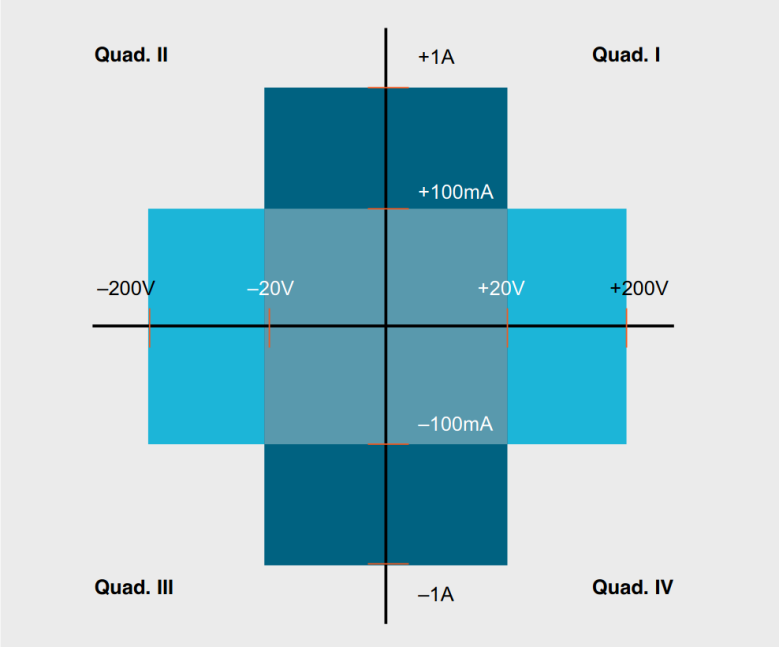

Figure 14: 2450 SMU power envelope. From [12]. The power supply can output a maximum effect of 20 W, however, this is not limited by the internal electronics, but in the software of the device, which only allows 100 mA of current if the voltage rises above 200 V

It is worth noting that the 2450 SMU is designed for very low-current applications, and so the probes are *tri*axial, not coaxial. This means that in addition to having the shield and the core, they have an inner shield, called the *guard*, which follows the voltage of the core. This is so that current leaks from the guard to the shield, not the core.

This is not a concern for this application, as the currents are quite large, additionally, the triaxial BNC connector has a slightly different layout, making it incompatible with the Attocube® patch board. To mend this, we use a connector which leaves the shield hanging and outputs only the shield and the core to a coaxial BNC connector.

- **Resistance**: The intrinsic resistance does not contribute to measurement error, but if the resistance of the system is too high, this will reduce the amount of current the SMU can deliver. If the output voltage climbs above 20 V, then the SMU will cap itself to 100 mA. In other words, the total resistance of the system must be kept below $\frac{20\,\mathrm{V}}{1\,\mathrm{A}} = 20\,\Omega$ if the experiment is to be done at the maximum current.

- **Current capacity**: The current capacity decides how strong a magnetic field can be generated and is decided primarily by two factors: The field strength generated per Ampére of current, and the amount of current which can be run through the stripline without melting it.

  This can be tested by increasing the current until the stripline melts, although it will not be entirely accurate. The switching time of a nanomagnet is very low, and so, the current can be supplied for a very short time. This would not give the stripline time to heat up, which means that a greater current can be supplied.

  Most applications will probably not use a constant power supply, but most likely either a single pulse or some pulsed digital signal. The current capacity will have to be tested depending on the desired input signal.

- **Field strength**: The field strength of a device is typically measured using a specialized tool, however, these structures are much too small to do this.

  One way of measuring the magnetic field strength at these small scales is to use the nanomagnets as indicators of the field strength. We know that the nanomagnet will flip at approximately 46 mT, and so, one can increase the current gradually while inspecting the nanomagnets in the MFM to determine whether the magnets have flipped.

  This introduces the risk of burning out the stripline before being able to measure the strength, so additionally, a bias field can be applied across the stripline. This can be safely increased until the magnets flip, and then lowered by a small known amount, for example 5 mT. Since the current required to generate this field is very small, there is no risk of destroying the stripline.

3.6 Simulations

Comsol is a program for simulating many kinds of different physical models and their interactions. For our purposes, this means modules for simulating Joule heating, EM fields and electric currents. Additionally, there is a CAD module which allows us to create models of striplines of different dimensions and run the simulations on them without supervision.

The result which we are primarily interested in is the amount of current required to generate the desired field strength. Additionally, it would be interesting to simulate the interaction between the resistive heating and the current, as resistance and temperature are related and affect each other, as discussed in chapter 2.5.

The setup we are using for the simulations are very simple. A rectangular gold wire, with a fixed width of 10 µm and height of 200 nm. Each simulation is run three times, one for each width of 2 µm, 10 µm and 20 µm.

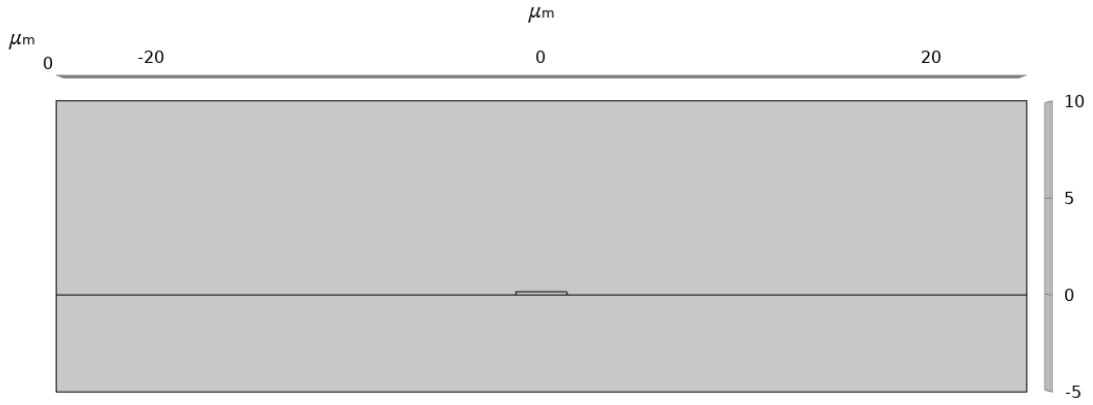

Figure 15: The model which will be used for simulations. The bottom layer is crystalline Si, while the top layer is helium. The stripline is simulated as a solid copper rectangle.

3.6.1 Practical considerations

The only real constraint for these simulations is the run time of the *study*. In this context, a study is a collection of simulations to run in Comsol under a given set of constraints. For example, a stationary study is a study which runs the simulation without time-dependent parameters, calculating the steady state result of a physics model.

In Comsol, studies that have time-dependent parameters are much more complex and time-consuming than those which have stationary time-independent solutions. As a result, simulating the Oersted field and the joule heating at the same time in a time-dependent study takes a very long time to run. This is due to the constant calculation of the resistance of the material based on the current temperature at the current position.

The run-time of the simulation can be improved greatly by fixing the resistivity of the metal, however, this means that we cannot simulate the feedback loop between resistivity and heating. As this is what is gained by simulating the heating and magnetic field together, there is no reason to do it.

Instead, two separate studies will be run, one to simulate the strength of the magnetic field for a range of currents, and one to simulate the heat generation for a range of currents over time.

3.6.2 Reliability of results

Although Comsol is a verified tool which can be very accurate, this is known until the results have been verified. Depending on the setup, there may be many unknowns which affect the results.

For the magnetic field generation, the primary risk is the influence of nearby measurement equipment, however, as the scale of the magnetic field is so small, the field has dropped off significantly by the time it reaches any other nearby structures. As there are few unknown variables which might affect the results, we expect this study to be quite accurate.

The heat generation study has multiple unknown variables which almost certainly will affect the results. The amount of heat generated is most likely accurate, however, it is not known how much of this is dissipated through the air and sample holder. This will lead to a build-up of heat which settles at a higher or lower temperature than in reality.

4 Results & discussion

4.1 Simulation results

4.1.1 Magnetic field simulations

To simulate the field strength, we apply a known current through the stripline by applying a virtual terminal to each end of it through the MEF module. The magnetic field strength is simulated using equation 3 on differential form.

For convenience, simulation results for a stripline of width 2.63 µm have been added after the fact, so that it can be compared with the fabricated stripline.

The field strength drops off with distance, so the field will be weaker at the top of the nanomagnets than at the bottom, however, the thickness of the magnets is only 12.5 nm, which should not significantly impact the field strength, as can be seen in figure 16

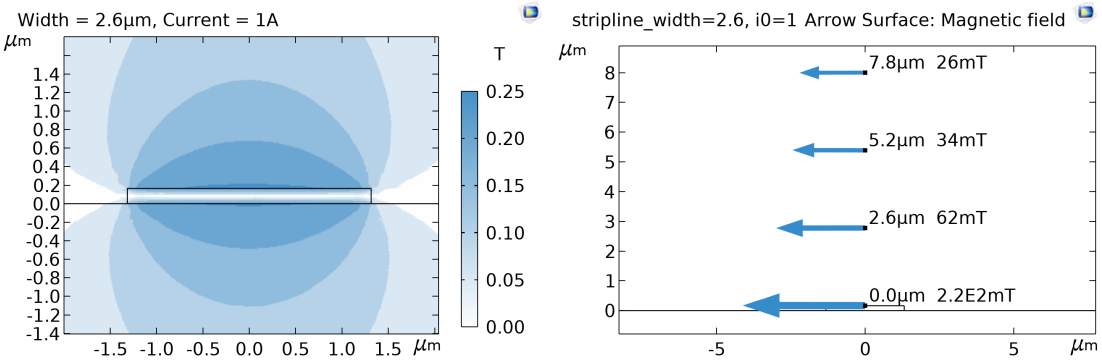

Figure 16: Cross sections of the stripline. Left a close-up surface contour plot of the field strength in x-direction. The Y-axis starts at the substrate. Right a macroscopic view of the field strength drop-off. The Y-axis starts at the stripline surface. At the center of the stripline, the field strength is at full strength until roughly 35 nm above the surface.

The results from the simulations are shown in figure 17, where the magnetic field strength is measured across the stripline at a height of 1 nm above the stripline.

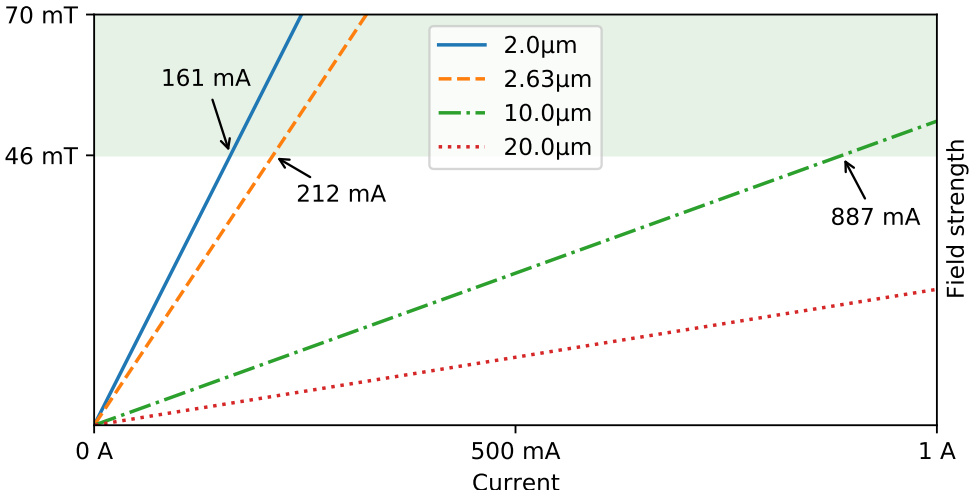

Figure 17: Plot of the magnetic flux across the stripline against the input current for four different widths

We see that there is a linear correlation between the simulated current and the field strength, and in general, a larger width is indicative of a weaker field. This is reasonable, as the surface area is larger, but the current is the same.

4.1.2 Temperature simulations

The temperature development was simulated using the AC/DC module combined with the Joule heating module. A current source and a ground node was attached to the stripline, and the temperature at the bottom of the substrate and top of the air was fixed at 300 K

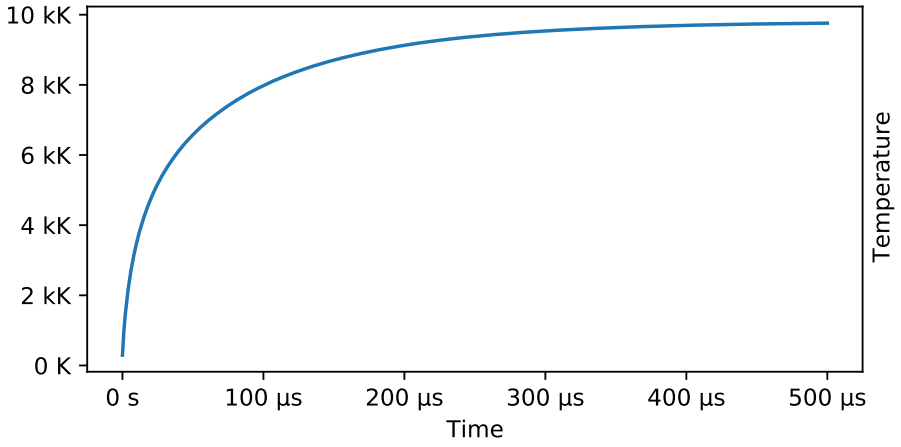

Figure 18: Plot of the temperature over time at a current of 212 mA for a stripline with a width of 2.63 µm, measured in the center of the stripline. After approximately 300 µs, the temperature has stabilized at a little under 10 kK.

This is clearly not an accurate result. It is obvious that there is no way to heat a copper wire to 10 kK by passing current through it, as this is much higher than the melting point of copper.

This result is primarily due to the fact that the heat flux out of the system is unknown. This could be tested experimentally, after which the simulations could be calibrated, however, as the temperature development does not need accurate characterization for this project, it is beyond the scope of this work.

The heat output is still important, as it determines the maximum current capacity, however, this will be tested physically instead of in simulations.

4.2 Sample fabrication

The samples were created at NTNU NanoLab[13], for a printable compact version of the process steps, refer to appendix A.

4.2.1 Stripline layer

The stripline layer was made using a relatively standard lithography process, as the structure is both simple and large. The main challenge in this process is the width and smoothness of the stripline. If it is too wide, the magnetic field might not be strong enough, if it is not smooth enough, the nanomagnets might not bond properly to the stripline.

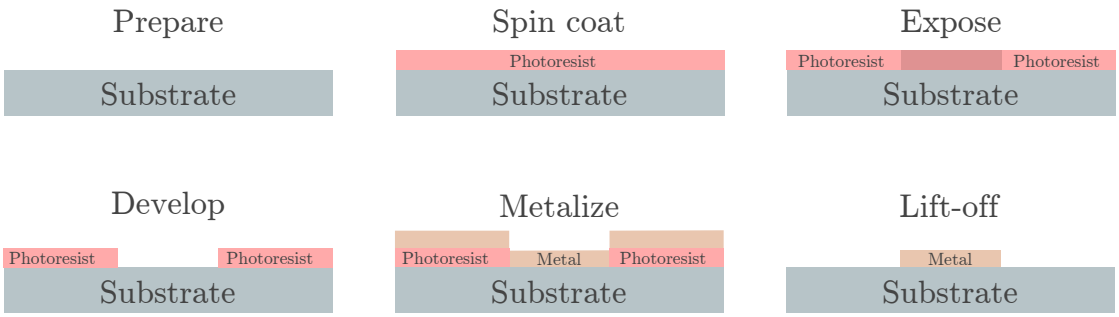

Figure 19: The process steps for manufacturing the stripline layer. Illustrated as a cross section of the wafer.

A 2″ 250 µm thick wafer was used. These wafers are initially quite clean, however, it is good practice to always clean them. The cleaning was done by submerging the wafer in acetone for around a minute, and then quickly transferring it to a beaker of isopropanol (IPA) while rinsing with a squirt bottle of IPA. The IPA should be dried off by holding one of the wafer edges to a lint-free cloth and blow drying with nitrogen, so that the cloth absorbs it.

Acetone is an excellent polar solvent, and cleans off most contaminants, but it evaporates very quickly, which might deposit the contaminants back onto the wafer. As IPA is a non-polar solvent, it both cleans off any remaining contaminants not yet dissolved, as well as any remaining acetone. To finalize the cleaning process, the wafer is plasma cleaned with oxygen for five minutes at maximal effect. This ensures a smooth, clean surface on which the photoresist can be spin-coated.

Prior to spin-coating, the wafer has to be baked to remove all moisture from the surface, this was done by baking at 150 °C for 5 min. A positive photoresist, SPR700[14], is spun on at 4000 rpm for 30 s, with acceleration set to 1000 rpm/s. This leads to a layer which is approximately 1 µm thick. A short soft-bake at 95 °C for 1 min evaporates some of the solvent, which hardens the resist.

The first exposure is done using the Heidelberg maskless aligner (MLA) 150[15]. This machine has a lower resolution than the Elionix EBL system, but it is significantly faster, and will be able to correctly expose the 2 µm stripline. The only structures that are too small for the MLA are the inner crosses of the alignment marks. This might be a problem when aligning for later exposures, but did not become an issue with this sample, as alignment using the square is still possible.

After a 1 min post-exposure bake (PEB) at 115 °C, the wafer is developed in a mixture of 70% MA-D 332[16] to 30% distilled water (DIW) for 40 s, before being *descummed* in the plasma cleaner for 30 s to remove the remaining organic residue from the top layer.

The sample can now be metalized. The primary current carrier is Cu, as it is cheap and very conductive, but it has some drawbacks. The adhesion to Si is not very good, and it oxidizes quickly at high temperatures, at which point it no longer carries current. To improve adhesion, a 5 nm layer of Ti is deposited first, then 145 nm copper, and then 10 nm Al to protect from oxidization. This is done in the Kurt J. Lesker E-beam evaporator[17] at respectively 3 Å/s, 5 Å/s, and 2 Å/s. The metal layers are illustrated in figure 20.

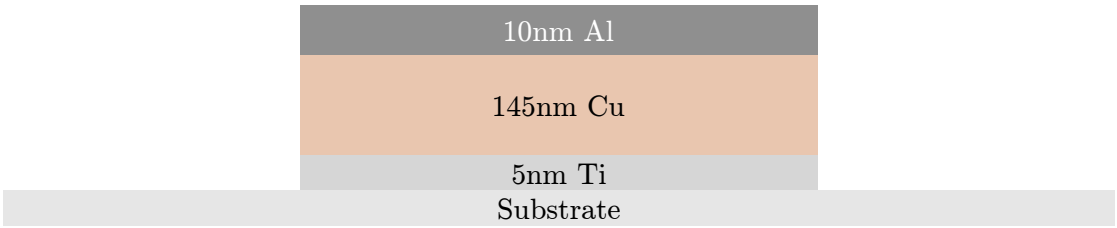

Figure 20: Illustration of a cross section the metal layers deposited using the lesker E-Beam evaporator. Not to scale.

To remove the surplus resist and metal and finalize the stripline layer, lift-off was done in acetone in an ultrasonic bath for ten minutes.

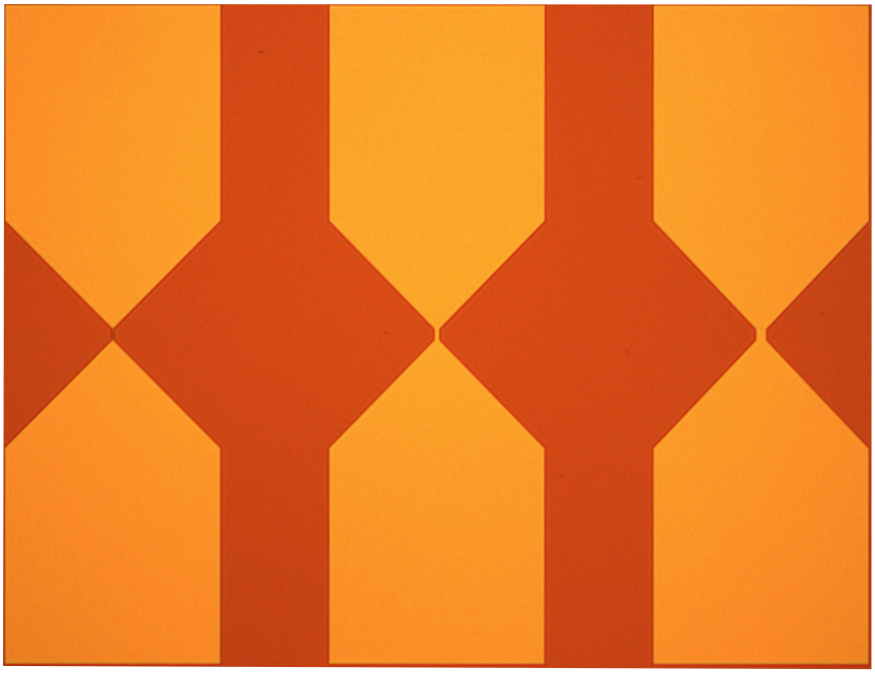

Figure 21: 5 times amplified optical image of structures made using this process. Three striplines with widths of 2 µm, 10 µm and 20 µm and a length of 10 µm. These are not the striplines which will be used, but have been made with the same process

This process resulted in a stripline which was slightly wider than 2 µm, but otherwise without defects. As noted earlier, the inner alignment marks are too small for the MLA, however, alignment is still possible without significant difficulties. See figure 22.

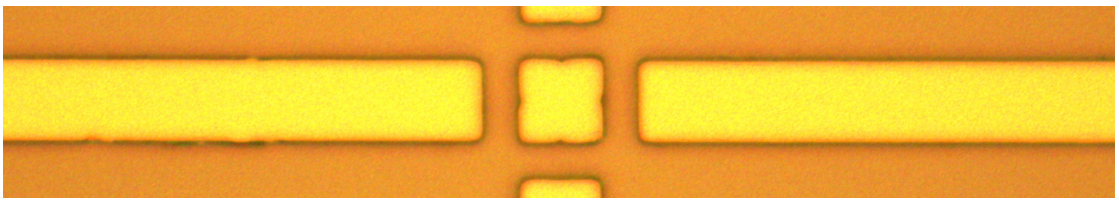

Figure 22: 100 times amplified optical image of the metalized alignment mark. Ideally, the four notches on the inner square would be grooves, leading to an additional inner cross

4.2.2 Nanomagnet layer

The cleaning process was repeated before beginning with the nanomagnet layer, however, with a shorter plasma clean. If the surface is improperly cleaned, there might be insufficient adhesion between the Ti and Py, which could cause some or all of the nanomagnets to fall off the stripline.

The resist used for this layer was a diluted solution of CSAR 62 (AR-P 6200.09)[18] with a ratio of 1:1 CSAR 62 to anisole. Spinning was done in two steps, first a 3 s ramp up to 500 rpm with an acceleration of 200 rpm/s, and then a 60 s spin at 8000 rpm/s with an acceleration of 1000 rpm, followed by a soft bake at 150 °C for 1 min. This was not to get a very low thickness, but to ensure that the resist had enough force to climb up and over the structure.

The second layer was exposed using the Elionix[19] EBL system at a rate of 500 pA. Although the inner crosses of the alignment marks were not fully exposed, there were no problems with alignment.

10 nm Py and 2.5 nm Ti were deposited using the Pfeiffer E-Beam evaporator. While depositing the Py-layer, the current held stable at roughly 36.5 mA and a rate of 1.8 Å/s. The final layer, which is a Ti-layer, was deposited with a current of roughly 116 mA and 1.2 Å/s. The final layer structure is illustrated in figure 23

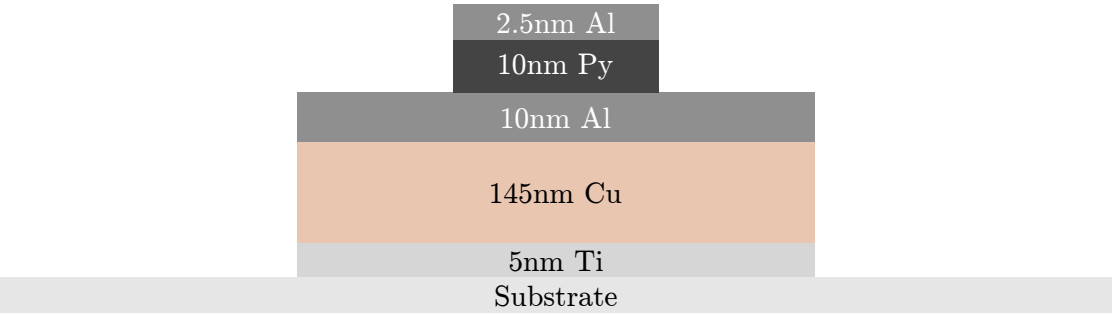

Figure 23: Cross section illustration of the metal layers deposited using the Lesker and the Pfeiffer. Not to scale.

The resist was stripped using AR600-71 for approximately 10 minutes. Initially no ultrasound was used, to avoid any possibility of the nanomagnets falling off the stripline, however, this resulted in poor dissolution, and eventually mild ultrasound was used.

4.3 Inspection & measurement

A wafer with 9 chips, each with 4 striplines were made at NTNU Nanolab. All were inspected optically and given a score from 1-9, which yielded a total of 5 chips without defects, 2 chips with visible impurities on one or more of the nanomagnets, and 2 chips with missing magnets on one or more of the striplines.

During inspection, it was noticed that the samples seemed to have some sort of residue near the edges of the stripline, which was then investigated in the scanning electron microscope (SEM).

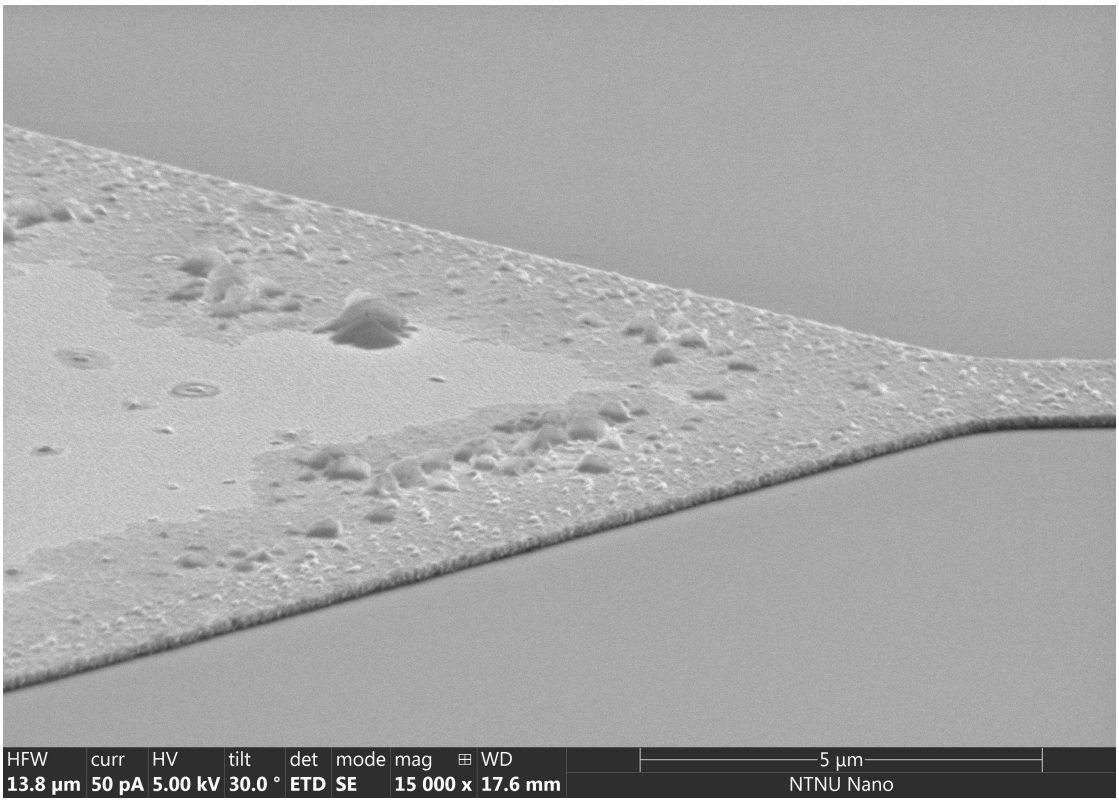

Figure 24: A SEM image of the are where the contacts taper into the stripline. Note that the crud seems to primarily stick to the edges of the stripline.

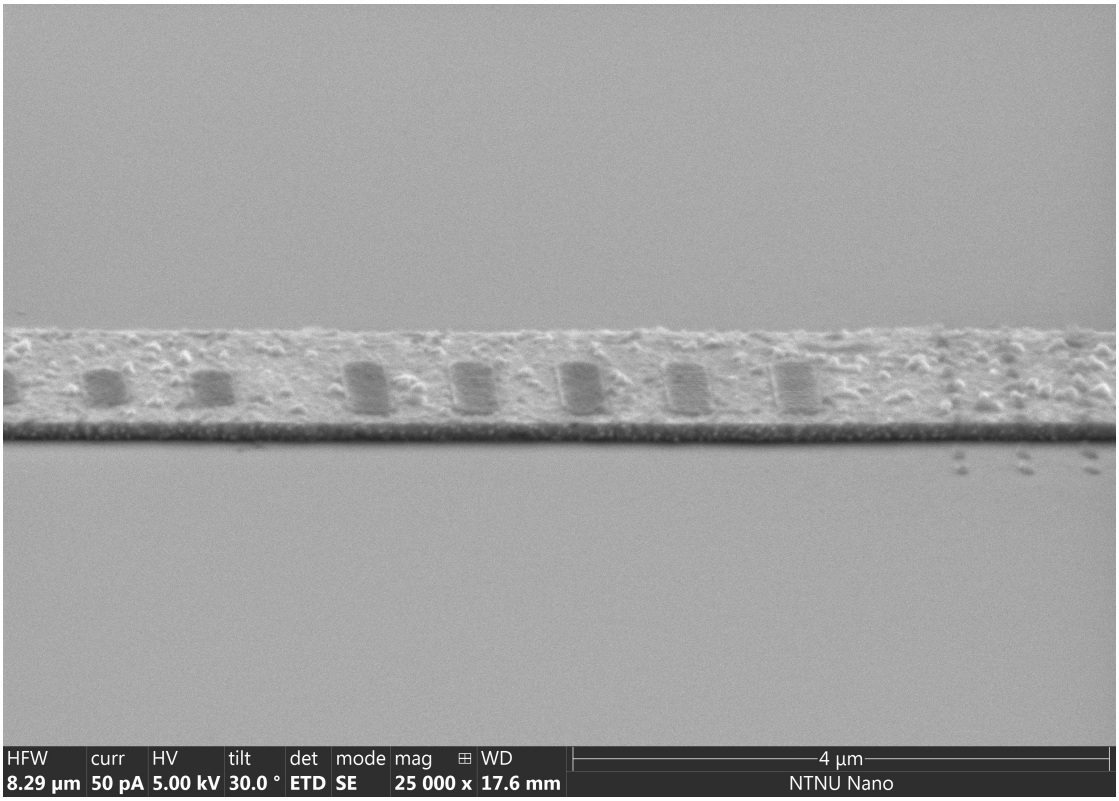

Figure 25: A SEM image close-up of the stripline. A set of large nanomagnets are visible, as well as scattered bits of crud.

This was initially thought to be an unknown organic residue from the manufacturing process.

This was tested by plasma cleaning and stripping. One chip was plasma cleaned with 50% O_2 at 50% power for 30 s at a time. After 2.5 min, this had no obvious effect. Another chip was placed in AR600-71 to strip any remaining resist for 15 min, before being cleaned with acetone and IPA. When this had no effect, this was done for another 15 min.

The stripped chip was then plasma cleaned, and vice versa, which did not have any obvious results either. This indicates that the residue was some sort of metallic compound.

Exactly what caused the residue to deposit on the stripline is uncertain. There are times when metal redeposits after lift-off, however, this is would most likely affet the whole stripline similarily. As seen in the SEM image in figure 24, the substrate and center of the stripline are relatively clean, which indicates that this is something related to the edges of the stripline.

A possibility is that this relates to the thickness of the resist. The layer is initially only approximately 100 nm thick. At the edges, the resist might have been even thinner, as illustrated in figure 26, allowing some of the metal to penetrate.

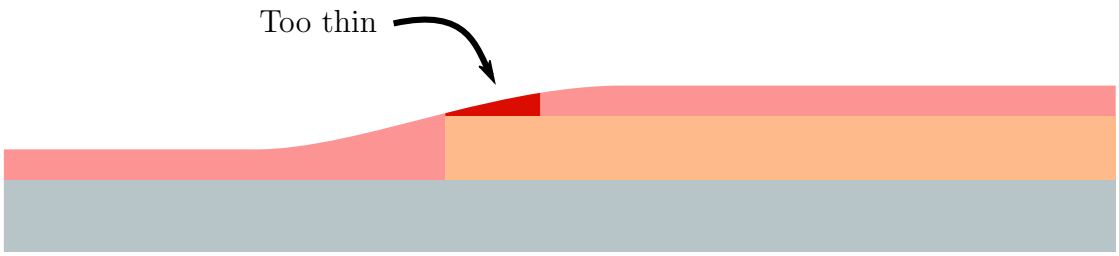

Figure 26: Illustration of possible cause of crud along the edge of the stripline. As the resist pushes up against the stripline and flows over, it might not coat the edges with a sufficient thickness

This would explain why the resisdue is seen primarily along the edges, but not why there are impurities on the sides of the stripline as well.

4.4 Measurements

For measuring in MFM and AFM, one of the samples was wire-bonded into a holder for the Attocube® AFM/MFM and mounted in the cryostat. Inspection using AFM was extremely difficult due to the amount and size of the crud.

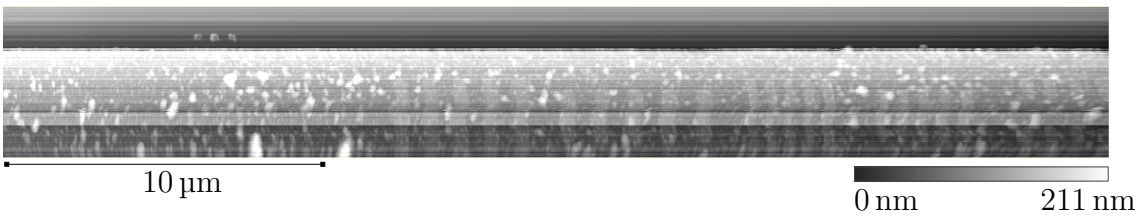

Figure 27: AFM heightmap of roughly half of the width of the stripline. The nanomagnets are visible, however, due to some very large crud, their relative intensity is quite low.

The AFM measurements are used primarily to locate the striplines on the samples, as this is much harder using MFM since only magnetic materials can bee seen with it. Once the stripline has been located, the instrument can be instructed to measure only a small region with greater resolution, for example a small group of nanomagnets, as shown in figure 28

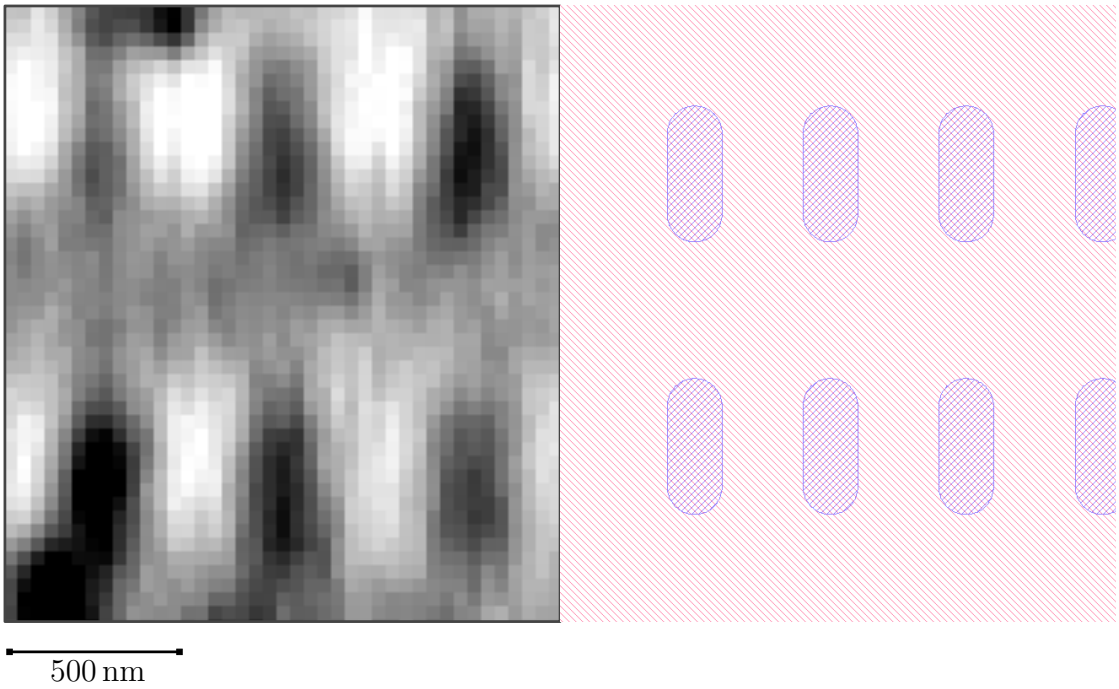

Figure 28: Left MFM image of a small group of nanomagnets with 100 mT bias field applied south to north. Reversing the field had no effect. Right CAD layout for the nanomagnets.

Note that the magnetization direction in figure 28 is not as expected. We should see a dark spot at the southern end and a bright spot at the northern end, instead the stray field appears to be directed into the plane, or sideways across the nanomagnets.

This further reinforces the idea that this is a metallic compound, as it seems to have a large impact on the overall stray field of the sample. This also means that the magnetic field simulations cannot be verified with this sample.

As noted earlier, the values which are of interest are:

- Resistance: The total resistance of the system must be kept low enough that the SMU can supply sufficient current, below 20 Ω to supply the full 1 A.

- Current capacity: The maximum current the stripline can sustain without melting
- Field strength: The magnetic field strength generated per Ampére of current.

Due to state of the stripline surface, the field strength cannot be characterized, so for calculation of example values, the results from the simulations will be used.

We can find the intrinsic resistance of the system by measuring the resistance of a sample outside the system, and the total resistance of the system with the sample mounted. Using a sample with $R \approx 0.5\,\Omega$ we measure the resistance of the total system to be around $55.6\,\Omega$ for the 3DR, and $7.3\,\Omega$ for the MFM holder, which means that the resistance of the measurement equipment is roughly $55\,\Omega$ and $6.8\,\Omega$ respectively. As the SMU will not supply more than 20 V, this means that the maximum current is $\frac{20\,\mathrm{V}}{55\,\Omega} \approx \underline{360\,\mathrm{mA}}$ in the 3DR holder, while a full Ampére can be supplied in the AFM holder.

Based on the results from the simulations, this effectively limits the width of the stripline in the 3DR, as both the 10 µm and 20 µm stripline needs a higher current to supply an adequate magnetic field. The 2 µm stripline can generate a field of roughly 70 mT at 360 mA, which is more than enough.

The current capacity was found by running a slow sweep from 1 mA to 1 A. The sweep has to be slow enough that the temperature will stabilize before increasing the current further. In the 3DR, the current cannot surpass 360 mA due to the resistance of that measurement system. At that current, the stripline never burned out.

In the MFM/AFM holder, the resistance was only $7.3\,\Omega$, which means that the current can be raised up to 1 A. The stripline burned out at approximately 600 mA. At this current, the field strength should be approximately 360 mT, which gives a field strength per current of 230 mT/A.

5 Conclusion & further work

Magnetic field simulations were performed in Comsol, which indicated that a stripline with micrometer dimensions could be fabricated so that a reasonable current would create a magnetic field of sufficient strength to switch nanomagnets in an ASI.

The fabricated stripline had had dimensions of 100 µm × 2.6 µm × 165 nm. This stripline could carry approximately 600 mA of current before melting, which the simulations indicate will produce a field of approximately 360 mT. However, due to fabrication challenges, this was never verified.

A natural next step is to investigate the cause of the surface impurities, as it is currently not known why this appeared. It might be as simple as using ultrasound immediately during stripping, but it might also be due to some unknown reaction between, for example, the stripper and one of the metal interfaces in the stripline. It is possible that this obstacle can be overcome by adjusting the spin-coating method. A more viscous resist, slower spin, or multi-layering the resist might affect the outcome, but due to the uncertainty around the cause, it is hard to speculate without further experimentation.

This project only examined a stripline with nanomagnets directly on top as this is very directly related to applications in ASI, however, there are other designs which might be relevant. For the measurement of the magnetic field, one could forego the nanomagnets altogether and use the anisotropic magnetoresistive effect, as illustrated in figure 29.

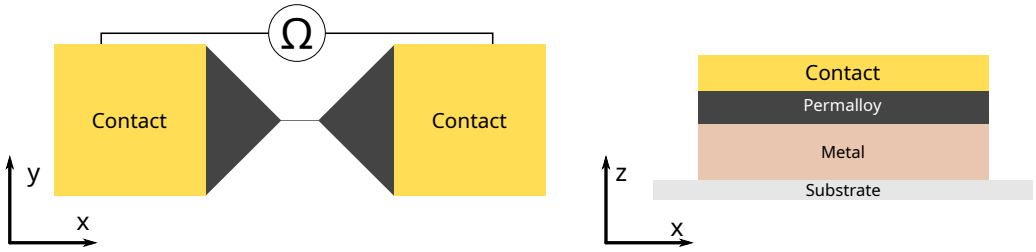

Figure 29: Illustration of a possible structure for using AMR for measuring the nanomagnets. A layer Py is deposited directly onto the stripline, and an ohmmeter is contacted across it. and as the resistance of the material changes with the magnetization direction, this can be used to measure the strength of the magnetic field.

The would have the advantage of allowing the layer of Py to be very large, even the entire width of the stripline, so long as contacts can be made for it. This means that one could fabricate the entire structure (except for the contacts) in only one lithography step, removing the need for the EBL and thus, the crud, entirely.

It appears that the use of a stripline as a means of switching nanomagnets in an ASI appears to be feasible, but further development of the fabrication method is required to achieve satisfactory results.

References

[1] Amanda Langørgen. "Magnetic Force Microscopy and Micromagnetic Simulations of Nanoscale Magnetic Structuresand Modified Artificial Spin Ices". MA thesis. June 2020.

[2] Turab Lookmana and Xiaobing Ren. *Frustrated Materials and Ferroic Glasses*. Springer Nature Switzerland AG, 2018. ISBN: 978-3-319-96914-5.

[3] Sandra Skjærvø et al. "Advances in Artificial Spin Ice". In: *Nature Reviews Physics* 2 (Nov. 2019). DOI: 10.1038/s42254-019-0118-3.

[4] J. M. D. Coey. *Magnetism and Magnetic Materials*. Cambridge University Press, 2010. ISBN: 978-0-521-81614-4.

[5] Lifeng Yin et al. "Magnetocrystalline Anisotropy in Permalloy Revisited". In: *Physical review letters* 97 (Sept. 2006), p. 067203. DOI: 10.1103/PhysRevLett.97.067203.

[6] Yannis Lever. "Towards Anisotropic Magnetoresistance Measurements in Artificial Spin Ice". MA thesis. June 2020.

[7] Andrew Cunningham and Nicholas Jardine. *Romanticism and the Sciences*. Cambridge University Press, 1990.

[8] Charles Byrne. *A Brief History of Electromagnetism*.

[9] Sergio Lupi, Michele Forzan, and Aleksandr Aliferov. *Induction and Direct Resistance Heating*. 1st ed. Springer, Cham, 2015. ISBN: 978-3-319-03479-9.

[10] Hugh D. Young and Roger A. Freedman. *University Physics*. 13th ed. Pearson, 2012. ISBN: 978-0-321-69686-1.

[11] Theodore C. Hennessy. *Lithography: Principles, Processes and Materials*. Nanotechnology Science and Technology. Nova Science Publishers, Inc, 2011. ISBN: 9781617618376. URL: http://search.ebscohost.com/login.aspx?direct=true&db=nlebk&AN=367184&site=ehost-live.

[12] *2450 SourceMeter® SMU Instrument Datasheet*. Keithley®. URL: https://download.tek.com/datasheet/1KW-60904-2_2450_Datasheet_020321.pdf.

[13] NTNU Nano. *NTNU NanoLab*. URL: https://www.ntnu.edu/nano/nanolab.

[14] Microresist Technology. *MICROPOSIT™ SPR™ 700 series*. URL: https://www.microresist.de/en/produkt/microposit-spr-700-series/ (visited on 05/23/2021).

[15] Heidelberg Instruments. *MLA150*. URL: https://heidelberg-instruments.com/en/products/mla150.html (visited on 05/23/2021).

[16] Microresist technology. *MA-D 332 aqueous-alkaline based devloper for photoresists*. URL: https://www.microresist.de/en/produkt/ma-d-332/ (visited on 05/30/2021).

[17] Kurt J. Lesker Company. *PVD75 PRO-LINE Thin Film Deposition System Platform*. URL: https://www.lesker.com/newweb/vacuum_systems/deposition_systems_pvd_prolinepvd75.cfm (visited on 05/23/2021).

[18] Allresist GmbH. *E-Beam Resist AR-P 6200 series (CSAR 62)*. URL: https://www.allresist.com/portfolio-item/e-beam-resist-ar-p-6200-series-csar-62/ (visited on 06/05/2021).

[19] STS Elionix. *ELS-G100 HIGH PERFOMANCE 100 KV LITHOGRAPHY SYSTEM*. URL: https://sts-elionix.com/product/els-g100/ (visited on 05/30/2021).

[20] TPT. *HB05 Wire Bonder*. URL: https://www.tpt-wirebonder.com/hb05/ (visited on 06/07/2021).

Appendices

A Process sheet

Step	Description	Tools
Wafer cleaning	Clean the wafer in acetone and rinse with IPA, blow dry with nitrogen. Plasma clean with 100% O_2 at 100% power for 5 minutes.	Diener Electronics Femto
Dehydration bake	Bake at 150 °C for roughly five minutes	EMS dual hot-plate
Spin coat	Spin coat the wafer with SPR700[14] for 30 seconds at 4000 rpm with 1000 rpm/s acceleration	Hirschmann opus spin coater
Soft bake	Bake at 95 °C for 1 minute	EMS dual hot-plate
Exposure	Expose the pattern with a dose of 110 J/cm^2	Heidelberg MLA 150[15]
PEB	Bake at 115 °C for 1 minute	EMS dual hot-plate
Development	Develop using MA-D 332[16] for 40 seconds while stirring, rinse with distilled water	
Descum	Plasma clean with 50% O_2 at 50% power for 30 seconds.	Diener Electronics Femto
Metalization	Deposit 5 nm titanium at 3 Å/s, 145 nm at 5 Å/s, and 10 nm Al at 2 Å/s	K. J. Lesker E-Beam Evaporator [17]
Lift-off	Dissolve the resist with acetone. Use ultrasonic bath for agitation. Rinse with IPA and blow dry with nitrogen.	Ultrasonic bath
Wafer cleaning	Clean the wafer in acetone and rinse with IPA, blow dry with nitrogen. Plasma clean with 100% O_2 at 100% power for 2 minutes.	Diener Electronics Femto
Dehydration bake	Bake at 150 °C for 7 minutes	EMS dual hot-plate
Spin Coat	Spin coat with 1:1 w/w AR-P 6200.09 to anisol with two steps on the spinner, first a 3 s ramp up to 500 rpm with an acceleration of 200 rpm/s, and then a 60 s spin at 8000 rpm with an acceleration of 1000 rpm/s	Hirschmann opus spin coater
Exposure	Expose in the EBL with a beam current of 500 pA	Elionix ELS-G100[19]
Metalization	Deposit 10 nm Py and 2.5 nm Ti at rates of respectively 36.5 mA/1.8 Å/s and 116 mA/1.2 Å/s	Pfeiffer E-Beam evaporator
Lift-off	Perform lift-off in AR600-71 with mild ultrasound agitation. Rinse with acetone and IPA	Ultrasonic bath
Scribing	Scribe into chips of suitable sizes for mounting in an LCC or AFM/MFM sample holder. Roughly 4 mm × 4 mm	Suss MicroTec scriber
Wire-bonding	Wire-bond to an LCC or AFM/MFM sample-holder.	TPT HB05 Wedge and Ball Bonder[20]

Table 4: Summary of sample fabrication process

B Images from production process

B.1 Metalization

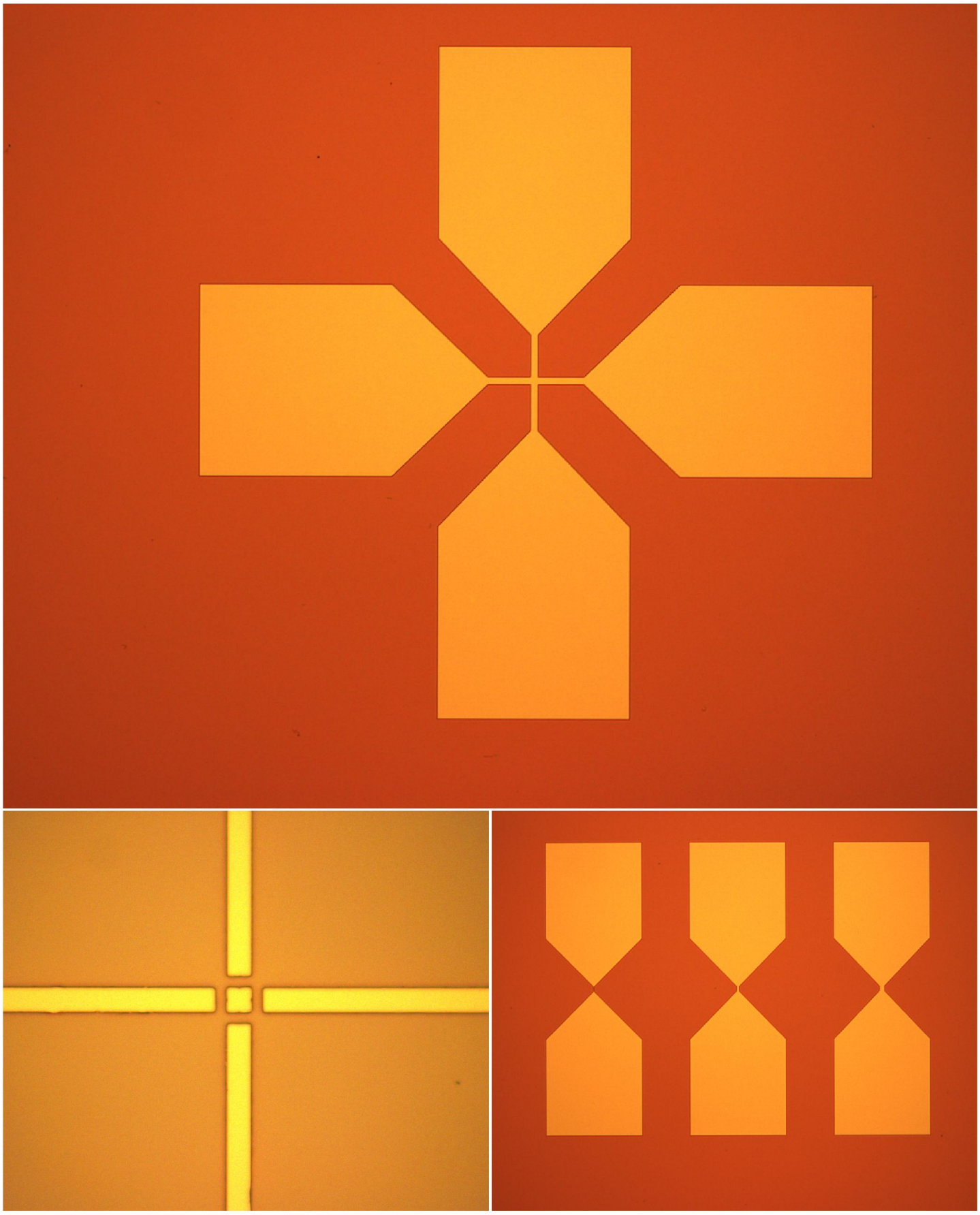

Figure 30: Top: Optional design which allows for magnetic fields in diagonal directions. Bottom left: Alignment mark. Bottom right: Macro image of a collection of 3 striplines with widths of 2 µm, 10 µm and 20 µm

B.2 EBL Exposure

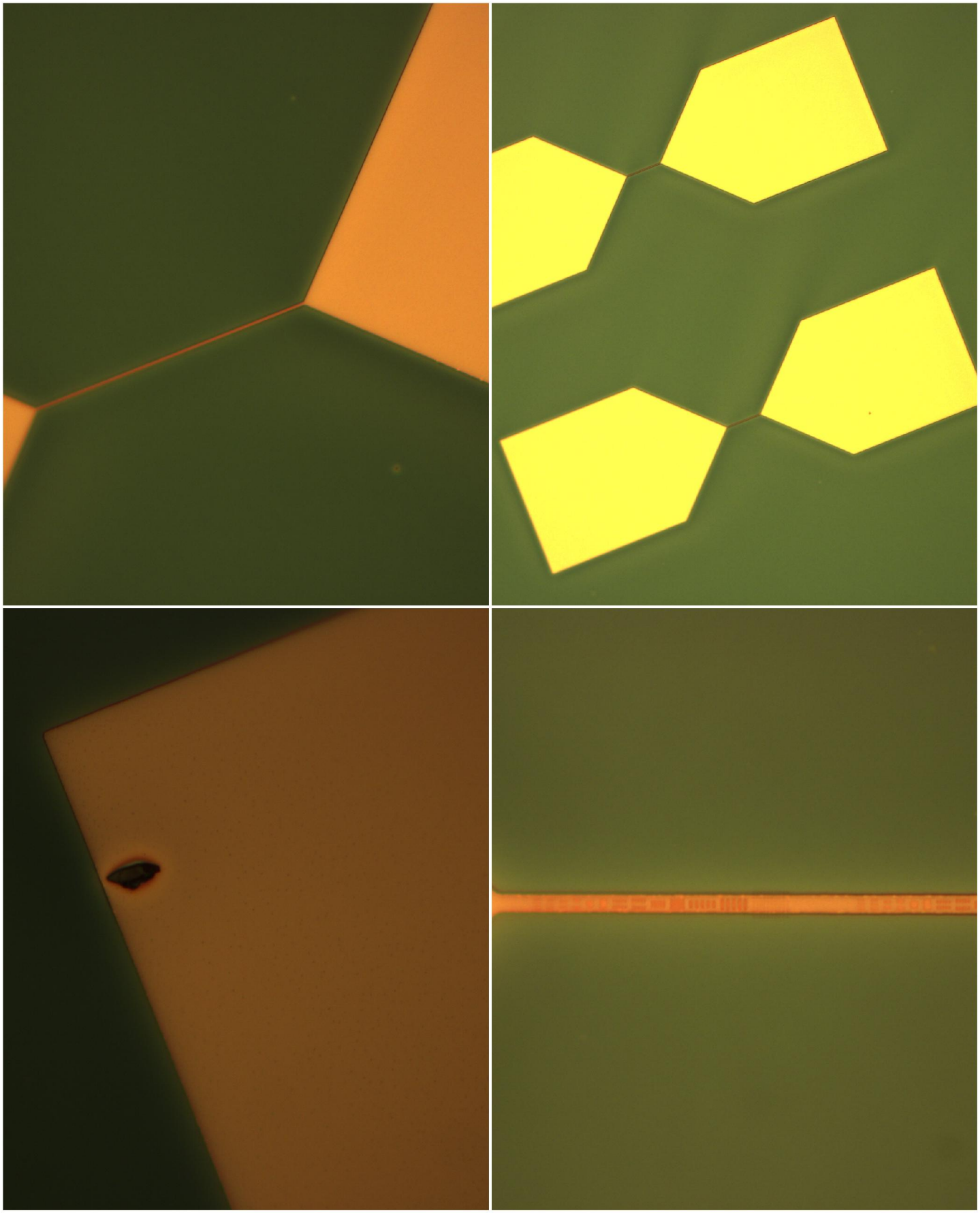

Figure 31: Top left: Single coated and developed stripline. Top right: Macro view of striplines coated with CSAR resist and exposed. Bottom left: Impurity on one of the contacts. Bottom right: 100x amplification of single stripline with visible nanomagnet pattern.

NTNU

Norwegian University of
Science and Technology